

Late summer sea ice segmentation with multi-polarisation SAR features in C- and X-band

A. S. Fors et al.

Late summer sea ice segmentation with multi-polarisation SAR features in C- and X-band

A. S. Fors¹, C. Brekke¹, A. P. Doulgeris¹, T. Eltoft¹, A. H. H. Renner², and S. Gerland³

¹Department of Physics and Technology, University of Tromsø – The Arctic University of Norway, 9037 Tromsø, Norway

²Institute of Marine Research, 9294 Tromsø, Norway

³Norwegian Polar Institute, FRAM Centre, 9296 Tromsø, Norway

Received: 30 June 2015 – Accepted: 21 July 2015 – Published: 1 September 2015

Correspondence to: A. S. Fors (ane.s.fors@uit.no)

Published by Copernicus Publications on behalf of the European Geosciences Union.

Title Page

Abstract

Introduction

Conclusions

References

Tables

Figures

◀

▶

◀

▶

Back

Close

Full Screen / Esc

Printer-friendly Version

Interactive Discussion

Abstract

In this study we investigate the potential of sea ice segmentation by C- and X-band multi-polarisation synthetic aperture radar (SAR) features during late summer. Five high-resolution satellite SAR scenes were recorded in the Fram Strait covering iceberf-
5 fast first-year and old sea ice during a week with air temperatures varying around zero degrees Celsius. In situ data consisting of sea ice thickness, surface roughness and aerial photographs were collected during a helicopter flight at the site. Six polarimetric SAR features were extracted for each of the scenes. The ability of the individual SAR features to discriminate between sea ice types and their temporally consistency were
10 examined. All SAR features were found to add value to sea ice type discrimination. Relative kurtosis, geometric brightness, cross-polarisation ratio and co-polarisation correlation angle were found to be temporally consistent in the investigated period, while co-polarisation ratio and co-polarisation correlation magnitude were found to be temporally inconsistent. An automatic feature-based segmentation algorithm was tested
15 both for a full SAR feature set, and for a reduced SAR feature set limited to temporally consistent features. In general, the algorithm produces a good late summer sea ice segmentation. Excluding temporally inconsistent SAR features improved the segmentation at air temperatures above zero degrees Celcius.

1 Introduction

A decline in the Arctic sea ice extent has been observed during the last decades, together with a large reduction in sea ice thickness and sea ice volume (Kwok et al., 2009; Parkinson and Comiso, 2013; Laxon et al., 2013; Meier et al., 2014). The reduction in sea ice volume has also lengthened the melt season at a rate of about five days per decade since 1979 (Stroeve et al., 2014). To understand the processes governing
20 these changes, and to meet the needs of shipping, oil and gas industries in an increas-

TCD

9, 4539–4581, 2015

Late summer sea ice segmentation with multi-polarisation SAR features in C- and X-band

A. S. Fors et al.

Title Page

Abstract

Introduction

Conclusions

References

Tables

Figures

◀

▶

◀

▶

Back

Close

Full Screen / Esc

Printer-friendly Version

Interactive Discussion

ingly accessible Arctic, more detailed mapping and monitoring of the summer sea ice cover is required (Stephenson et al., 2013).

Synthetic aperture radar (SAR) is widely used in operational sea ice monitoring. The Canadian Ice Service alone processes ten to twelve thousand SAR images every year (Moen et al., 2013). Operating in the microwave frequency, SAR has the advantage of providing all-weather and day-night imagery. At present, operational sea ice services use single and dual polarimetric SAR images in sea ice monitoring due to their wide swath width and good temporal coverage. However, on a local scale, more information and improved sea ice segmentation can be retrieved from full polarimetric SAR imagery. Today, such data is in limited use mainly due to its reduced coverage. The recent development of compact polarimetry could open the way for more polarimetric radar information to be retrieved at larger swath widths (Raney, 2007; Dabboor and Geldsetzer, 2014).

C-band is considered the preferred frequency in operational sea ice satellite monitoring, offering a good all-season capability (Onstott, 1992). With the launch of TerraSAR-X (2007) and COSMO Skymed (2007) new opportunities in investigating the potential use of X-band (frequency of 9,6 GHz) in sea ice satellite monitoring appeared. Several studies have investigated the application of X-band radar for sea ice mapping through ground based, airborne and satellite borne platforms. X-band is found to have good separation capabilities between first-year ice and old ice (Onstott, 1992), between water and sea ice (Brath et al., 2013), and in detection of thin ice (Matsuoka et al., 2001). For the Baltic Sea, results show that the information content in C- and X-band are largely equivalent (Mäkynen and Hallikainen, 2004; Eriksson et al., 2010). X-band has been found to add information when used in combination with C-band (Brath et al., 2013).

Several techniques for automatic segmentation of sea ice in SAR scenes exist. Methods consist of thresholding of polarimetric features, gamma distribution mixture models, K-means clustering, neural networks, Markov random field models, Gaussian mixture models, Wishart classifiers and iterative region growing using semantics (see Moen

Late summer sea ice segmentation with multi-polarisation SAR features in C- and X-band

A. S. Fors et al.

Title Page

Abstract

Introduction

Conclusions

References

Tables

Figures

◀

▶

◀

▶

Back

Close

Full Screen / Esc

Printer-friendly Version

Interactive Discussion

et al., 2013, and references therein). Several of these methods are feature-based methods, making use of a feature set in the segmentation. They have the advantage of being flexible as the input features used can be varied with, e.g., location and seasonal conditions, and the features offer possible post-segmentation information as an interpretation and labeling source. Moen et al. (2013) showed promising results in segmenting a full polarimetric sea ice scene taken under winter conditions (low temperatures and snow cover) with a simple feature-based multi-channel SAR segmentation method described in Doulgeris and Eltoft (2010) and Doulgeris (2013), utilising six polarimetric features based on the covariance matrix.

Research has been conducted on SAR and microwave scatterometer measurements of sea ice since the early 1990s (Onstott, 1992). Most of the conducted studies have been in winter and late fall, and the number of studies in the melt period is limited. In winter, differences in salinity content and degree of deformation of sea ice make it possible to separate multi-year ice (MYI) and different stages of first year ice (FYI) from each other. During summer, more limited differences in salinity between MYI and FYI and the presence of moist snow and free water on the sea ice surface make monitoring with SAR challenging. Early studies on the use of SAR and microwave scatterometer data for summer sea ice applications can be found in, e.g., Onstott (1992); Gogineni et al. (1992); Carlstrom and Ulander (1993); Jeffries et al. (1997) and Yackel and Barber (2000). Newer studies include examination of backscatter signatures of multiyear sea ice with ship-based scatterometer (Isleifson et al., 2009), investigation of the use of a supplementary frequency of either X- or Ku-band in addition to C-band in late summer sea ice classification with an airborne scatterometer (Brath et al., 2013), the possibility of separating MYI and FYI by dual polarisation intensity data from Radarsat-2 (Warner et al., 2013), classification potential of polarimetric features from Radarsat-2 (Gill et al., 2013) and investigations of melt pond fraction retrieval from co-polarisation ratio data acquired by Radarsat-2 (Scharien et al., 2012, 2014b). Separating different sea ice types during summer-melt is still a challenge.

Late summer sea ice segmentation with multi-polarisation SAR features in C- and X-band

A. S. Fors et al.

[Title Page](#)[Abstract](#)[Introduction](#)[Conclusions](#)[References](#)[Tables](#)[Figures](#)[◀](#)[▶](#)[◀](#)[▶](#)[Back](#)[Close](#)[Full Screen / Esc](#)[Printer-friendly Version](#)[Interactive Discussion](#)

Late summer sea ice segmentation with multi-polarisation SAR features in C- and X-band

A. S. Fors et al.

Title Page

Abstract

Introduction

Conclusions

References

Tables

Figures

◀

▶

◀

▶

Back

Close

Full Screen / Esc

Printer-friendly Version

Interactive Discussion

The objective of this study is to investigate the potential of sea ice segmentation using C- and X-band multi-polarisation SAR features during late summer. A dataset consisting of five high resolution C- and X-band scenes recorded on iceberg-fast first-year and old ice in the Fram Strait in August and September 2011 is employed in our study.

5 The satellite data is combined with airborne measurements from a helicopter flight at the site. We explore how the features and feature-based automatic segmentation successfully employed on FYI during winter conditions in Moen et al. (2013) perform on late summer sea ice with temperatures around the freezing point. Our study consists of two parts: firstly, the suitability of the individual features for use in late summer sea ice segmentation is evaluated. This is done by investigating the ability of the individual features to discriminate between sea ice types and their temporal consistency during changing temperature conditions. A reduced set of the four most temporally consistent features is suggested for use in segmentation. Secondly, a feature-based automatic segmentation algorithm is tested on the dataset. The algorithm is tested both with a full feature set, and with the reduced feature set suggested in the first part of the study. The segmented images are evaluated both visually, and by pixelwise evaluation of regions with known geophysical properties.

2 Methods

In this study, we examine the potential of six polarimetric SAR features for use in late summer sea ice segmentation. To simplify the study, five regions of interest (ROIs) with different sea ice types are defined based on information from the satellite scenes and the helicopter flight at the site. The first part of this section describes the dataset utilized in our study. In the second part we explain the design of the study, including the choice of ROIs, the generation of polarimetric SAR features and the detailed methodology of the analysis.

2.1 Dataset

The data used in this study were collected from ship, helicopter and satellite during a coordinated campaign in the Fram Strait in late summer 2011. The dataset consists of several high resolution multi-polarimetric SAR scenes, together with airborne observations collected from a helicopter (Table 1). In addition, meteorological observations from the scientific vessel R/V *Lance* are also available, offering information about the changing weather conditions during the campaign. The area covered by the satellite scenes could not be reached by the ship, and the helicopter did not have the opportunity to land within the area, therefore no ground based in situ measurements from the sea ice surface were retrieved.

The study site is situated in an area with iceberg-fast sea ice located in the Fram Strait (see Fig. 1). Both first-year sea ice (FYI) and old sea ice in different stages of development are represented at the site.

2.1.1 Satellite measurements

For this study, three quad polarimetric C-band scenes from the Canadian Radarsat-2 (RS-2) satellite (denoted R1, R2 and R3) and two dual polarimetric X-band scenes from the German TerraSAR-X (TS-X) satellite (denoted T1 and T2) are used. More details about the scenes can be found in Table 1, and the position of the scenes are displayed in Fig. 1. All scenes are recorded in ascending orbits. The RS-2 scenes have a coverage of 25 km (range) \times 25 km (azimuth), while the TS-X scenes have a coverage of 15 km (range) \times 50 km (azimuth).

2.1.2 Air- and shipborne measurements

Airborne measurements were conducted during a helicopter flight out from R/V *Lance* within the period of the satellite campaign (see Table 1). They include sea ice thick-

Late summer sea ice segmentation with multi-polarisation SAR features in C- and X-band

A. S. Fors et al.

Title Page

Abstract

Introduction

Conclusions

References

Tables

Figures

◀

▶

◀

▶

Back

Close

Full Screen / Esc

Printer-friendly Version

Interactive Discussion



ness, relative surface roughness and classified aerial images. The track of the flight is displayed together with the location of the satellite scenes in Fig. 1.

2.1.3 Sea ice thickness

Measurements of total snow plus sea ice thickness (from now on referred to as sea ice thickness) were performed with an electromagnetic induction sounder (EM-bird), which was towed underneath the helicopter and flown at a height of about 15 m above the surface. More details about the EM-bird can be found in Haas et al. (2009); Renner et al. (2013, 2014). In this device, the difference in conductivity between sea ice and water is used to find the height of the EM-bird above the ice/water interface, and a laser altimeter integrated in the EM-bird detects the distance between the EM-bird and the snow/ice surface. The difference between the two measures gives the sea ice thickness. The footprint of the EM-bird has a diameter of about 50 m (depending on the height of the instrument). At the time of the acquisition there was very little or no snow on top of the sea ice.

2.1.4 Surface roughness

The data from the laser altimeter mounted on the EM-bird can be used to extract surface roughness (von Saldern et al., 2006; Beckers et al., 2015). Calibration is needed to remove helicopter altitude variations. This was done by the three-step high- and low-pass filtering method described in Hibler (1972). The resulting surface elevation profiles are relative to the level ice. Surface roughness is in this study presented as the standard deviation of the profile surface elevation about the mean (root mean square height), R_q ,

$$R_q = \sqrt{\frac{1}{N} \sum_{i=1}^N (y_i - \bar{y})^2}, \quad (1)$$

Late summer sea ice segmentation with multi-polarisation SAR features in C- and X-band

A. S. Fors et al.

Title Page

Abstract

Introduction

Conclusions

References

Tables

Figures

◀

▶

◀

▶

Back

Close

Full Screen / Esc

Printer-friendly Version

Interactive Discussion



where N represents the number of measurements, \bar{y} the mean height above level ice, and y_i the height above level ice of sample i . Each ROI profile is 400 m long, and N varies between 960 and 1067, depending on the speed of the helicopter.

2.1.5 Melt pond fraction

The helicopter was equipped with a digital camera (GoPro YHDC5170, focal length 5 mm, view angle 127°), taking downward looking photographs of the sea ice surface. The area covered by each image was about 85 m (length) \times 110 m (width) and the sampling rate was 0.5 Hz. The images were processed with a semi-automatic classification algorithm, separating classes of open water, submerged ice, melt ponds, very thin ice and thicker ice, as described in Pedersen et al. (2009) and Renner et al. (2013). The melt pond fraction, i.e., the percentage coverage of melt ponds retrieved from each image, is used in our description of the sea ice types in this study. No additional ground information could be retrieved about the state of the melt ponds at the site of the satellite scenes during the campaign; hence we do not know whether the melt ponds were open or refrozen at the time of the acquisitions. According to the cruise report, open melt ponds were observed during the first days of the cruise, but from 26 August a major part of the melt ponds had started to freeze over. Melt pond measurements in open melt ponds at the ice edge were however performed until 31 August.

2.1.6 Meteorological information

SAR scattering properties of sea ice are highly affected by temperature and humidity, and meteorological information can therefore aid the interpretation of SAR satellite scenes. Meteorological measurements were performed on the scientific vessel R/V *Lance* during the campaign (Fig. 2). R/V *Lance* was sailing during this period and its route was located in the Fram Strait within 100 km west and north of the position of satellite scenes. During the week of data collection, the weather conditions were varying and the temperature was fluctuating around zero degrees Celsius. We have no

Late summer sea ice segmentation with multi-polarisation SAR features in C- and X-band

A. S. Fors et al.

Title Page

Abstract

Introduction

Conclusions

References

Tables

Figures

◀

▶

◀

▶

Back

Close

Full Screen / Esc

Printer-friendly Version

Interactive Discussion



other areas of deformed ice can be seen as light-coloured regions in the right part of the scene possibly forming a shear ridge.

2.2.2 Polarimetric SAR features

Polarimetric SAR features combine information from the different channels of a multi-polarisation SAR system, and they represent information about the scattering properties of the surface. This study investigates the sea ice discrimination and segmentation potential of six polarimetric SAR features during changing temperatures in late summer. The features studied are previously successfully used in segmentation of a winter time sea ice scene (Moen et al., 2013). An overview of the features and their definitions is presented in Table 3. The features consist of relative kurtosis (RK) geometric brightness (B), cross-polarisation ratio ($R_{VH/VV}$), co-polarisation ratio ($R_{VV/HH}$), co-polarisation correlation magnitude ($|\rho|$) and co-polarisation correlation angle ($\angle\rho$). $R_{VH/VV}$ is used instead of $R_{HV/HH}$ as T2 has the polarisation combination VH–VV. By inspection, these two features show similar values in our dataset. $\angle\rho$ is equivalent to the more frequently used term co-polarisation phase difference (ϕ_{HH-VV}).

A full-polarimetric SAR system is transmitting and receiving both horizontal (H) and vertical (V) polarised electromagnetic waves, resulting in $d = 4$ possible polarimetric channels (S_{HH} , S_{HV} , S_{VH} and S_{VV}). Assuming reciprocity ($S_{HV} = S_{VH}$), the Lexicographic feature vector, \mathbf{s} , is given by (Lee and Pottier, 2009)

$$\mathbf{s} = [S_{HH} \sqrt{2}S_{VH} S_{VV}]^T, \quad (2)$$

where T denotes transpose. The covariance matrix, \mathbf{C} , is defined as the mean outer product of the Lexicographic feature vector (Lee and Pottier, 2009)

$$\mathbf{C} = \frac{1}{L} \sum_{i=1}^L \mathbf{s}_i \mathbf{s}_i^{*T}, \quad (3)$$

where \mathbf{s}_i is the single look complex vector corresponding to pixel i , L is the number of scattering vectors in a local neighbourhood and $*T$ denotes the Hermitian transpose. Hence, \mathbf{C} can be written as

$$\mathbf{C} = \begin{bmatrix} \langle S_{HH} S_{HH}^* \rangle & \langle S_{HH} S_{VH}^* \rangle & \langle S_{HH} S_{VV}^* \rangle \\ \langle S_{VH} S_{HH}^* \rangle & \langle S_{VH} S_{VH}^* \rangle & \langle S_{VH} S_{VV}^* \rangle \\ \langle S_{VV} S_{HH}^* \rangle & \langle S_{VV} S_{VH}^* \rangle & \langle S_{VV} S_{VV}^* \rangle \end{bmatrix}, \quad (4)$$

5 where the $\langle \cdot \rangle$ is the sample mean over L scattering vectors and $*$ denotes the complex conjugate.

The TS-X scenes included in our study are dual-polarmetric. The covariance matrix then reduces to a 2×2 matrix. This implies that the full feature set of six features could not be achieved for these scenes since the achievable feature set depends on the scenes' polarimetric channel combination (see Table 3). Note that RK and G in the TS-X scenes are calculated from reduced covariance matrices, and should not be directly compared to the similar RS-2 features.

10 $R_{VH/VV}$, $R_{VV/HH}$, $|\rho|$ and $\angle\rho$ are well known polarimetric features in sea ice applications (Drinkwater et al., 1992), while RK and B have seen less attention in the literature. RK is a measure of non-Gaussianity, and is defined as Mardia's multivariate kurtosis of a sample divided by the expected multivariate kurtosis of a complex normal distribution ($d(d+1)$) (Mardia, 1970; Douglgeris and Eltoft, 2010). $RK < 1$ points towards a distribution with broader shoulders and lighter tails than for Gaussian data, while $RK > 1$ implies a sharp peak close to the mean, and heavy tails relative to Gaussian distribution (DeCarlo, 1997). Large values of RK are expected for deformed sea ice due to scattering from a few strong reflections, and for inhomogeneous areas due to differences in intensity mixtures (Moen et al., 2013). B represents the intensity of the multichannel radar backscatter. It is closely related to the more familiar feature SPAN, i.e. $\text{trace}(\mathbf{C})$, as they both represent the eigenvalues of the covariance matrix. B is however more sensitive to the smaller eigenvalues.

Late summer sea ice segmentation with multi-polarisation SAR features in C- and X-band

A. S. Fors et al.

Title Page

Abstract

Introduction

Conclusions

References

Tables

Figures

◀

▶

◀

▶

Back

Close

Full Screen / Esc

Printer-friendly Version

Interactive Discussion



2.2.3 Data analysis

In the first part of our study, we examine the ability of the individual features to discriminate sea ice types, and their temporal consistency.

The sea ice type discrimination ability is evaluated through a maximum a posteriori (MAP) supervised classifier, using Baye's decision rule (Theodoridis and Koutroumbas, 2009). The classifier assigns pixel x to class ω_j if

$$P(\omega_j|x) > P(\omega_i|x) \quad \forall j \neq i. \quad (5)$$

where $P(\omega_j|x)$ is the probability of class ω_j given the feature value x . The probability density functions (pdfs) are estimated with a Parzen kernel density estimator, using a Gaussian kernel function (Theodoridis and Koutroumbas, 2009). The bandwidth used is a function of the number of points in the sample and their distribution, as described in Bowman and Azzalini (1997). As the ROIs investigated are relatively small, hence resulting in small sample sizes, leave-one-out cross validation is used in training and testing the classifier. A 7×7 pixels neighbourhood, $L = 49$, is used in the classification and a stepping window with steps of 5×5 pixels was employed to reduce neighbourhood overlap. The resulting classification accuracies obtained for each individual feature are used to evaluate the discrimination abilities of the features.

The temporal consistency of the individual features is studied qualitatively for the three RS-2 scenes, by inspecting the mean ROI values of each feature. We consider a feature temporally consistent if the ranking of the mean ROI values of the feature are similar in all three scenes. E.g., the ROI with the highest mean value for a specific feature has the highest mean value of that feature in all the three investigated scenes. Based on the result on temporal consistency, a reduced feature set of four features is suggested.

In the second part of our study, a feature-based automatic segmentation algorithm is tested on the five scenes in the dataset. It is tested both with the original full feature set, and with a reduced feature set excluding the most temporally inconsistent features. The

Late summer sea ice segmentation with multi-polarisation SAR features in C- and X-band

A. S. Fors et al.

Title Page

Abstract

Introduction

Conclusions

References

Tables

Figures

◀

▶

◀

▶

Back

Close

Full Screen / Esc

Printer-friendly Version

Interactive Discussion



segmentation uses Gaussian mixture models to model the features' pdf, and employs an expectation-maximization algorithm. Markov random fields are used for contextual smoothing. Further description of the segmentation approach is given in Doulgeris (2013) and Moen et al. (2013). A 21×21 pixels neighbourhood, $L = 441$, was used performing the segmentation. The large neighbourhood reduced the pixel resolution, but improved the results of the segmentation compared to a smaller neighbourhood, giving less granular segmentations. A stepping window with steps of 5×5 pixels was used to reduce neighbourhood overlap, and an additional sub stepping window of 10×10 pixels was used during the algorithm for computation efficiency. The algorithm was set to segment the scenes into six different classes, to allow for detection of the major sea ice types visually expected to be present in the scenes. For easier comparison, the area used in the segmentation is confined to the intersection of the individual scenes' geographical location (see the pink patch in Fig. 1). For each scene, the segmentation's performance is evaluated visually, and based on its ability to discriminate the pixels of the five ROIs into different classes.

3 Results and discussion

This section presents and discusses results from the two parts of our study. First, we examine the individual sea ice type discrimination ability and the temporal consistency of six polarimetric SAR features during changing air temperature conditions. Secondly, an automatic segmentation algorithm based on the investigated features is tested on the data set. Results for C- and X-band are presented separately, as differences in incidence angle, resolution and polarimetric channel combinations makes a direct comparison inappropriate (see Table 1). The features in C-band are based on the full covariance matrix, while those in X-band are based on reduced covariance matrices as the TS-X scenes are dual polarisation scenes (see Table 3). Note that ROI5 is only present in the RS-2 scenes.

Late summer sea ice segmentation with multi-polarisation SAR features in C- and X-band

A. S. Fors et al.

Title Page

Abstract

Introduction

Conclusions

References

Tables

Figures

◀

▶

◀

▶

Back

Close

Full Screen / Esc

Printer-friendly Version

Interactive Discussion



3.1 Discrimination ability and temporal consistency

In this section, we search for features that are suitable for use in late summer sea ice segmentation. We study both the ability of six individual features to discriminate sea ice types, and their temporal consistency during changing temperature conditions. Finally, we suggest a reduced feature set consisting on the four most temporally consistent features.

3.1.1 Discrimination ability

The sea ice type classification accuracies received from the supervised MAP classification are presented in Tables 4 and 5, for RS-2 and TS-X respectively. The presented values represent the diagonal values of the confusion matrices, i.e., the percentage of true classification. The best result for each ROI is highlighted in bold. All pixels from the five ROIs were included in the classification, and the experiment was performed separately for each of the scenes included in the study.

From the two tables we note that none of the features individually were able to classify all the five ROIs in a single scene with high accuracy. All features do however give satisfying classification results for some of the sea ice types represented by the ROIs, in some of the scenes. Hence, by combining the features, all features could add value to a feature-based sea ice type segmentation algorithm.

The best feature for discriminating a given ROI is varying from scene to scene. In all scenes except T1, ROI4 seems to be the most challenging to separate from the others. ROI4 consist of old ice, as does ROI3. An overlap between the pdfs of these two ROIs could be a reason for the poor discrimination result of ROI4.

In general, the result of the MAP classification for C- and X-band does not show large differences. The best classification accuracies in the C-band scenes are slightly higher than those in the X-band scenes, indicating a larger discrimination potential in C-band. This difference is not necessary a result of different frequency. RK and B is calculated from a reduced covariance matrix in the X-band scenes, and therefore contains less

TCD

9, 4539–4581, 2015

Late summer sea ice segmentation with multi-polarisation SAR features in C- and X-band

A. S. Fors et al.

Title Page

Abstract

Introduction

Conclusions

References

Tables

Figures

◀

▶

◀

▶

Back

Close

Full Screen / Esc

Printer-friendly Version

Interactive Discussion



information. Differences in incidence angle and resolution could also cause the lower accuracies in the X-band scenes.

3.1.2 Temporal consistency

The temporal evolution of the features' mean in each ROI is displayed in Figs. 6 and 7 for RS-2 and TS-X, respectively. The variances of the features within each ROI are displayed as error bars equivalent to two standard deviations. Due to different polarisation channel combinations (see Table 1), different features are displayed for T1 and T2 in Fig. 7. This also limits a temporal investigation in X-band, and we will in the following focus on the results in C-band.

As weather conditions and incidence angles are different for the RS-2 scenes in the dataset (see Table 1), the mean ROI values of the features is expected to vary between the scenes even if sea ice conditions would be the same or very similar. Hence, when searching for temporal consistent features, we look at the evolution of the ranking of the mean ROI values of each feature. For instance, studying RK in Fig. 6, the mean value within each ROI varies between the scenes. However, the relative relationship between the different mean values is almost constant. The RK of ROI5 does for instance take values between 1.05 and 1.15, but the RK value is always highest in this ROI. The same between-ROI-consistency during the investigated period can also be found for B , $R_{VH/VV}$ and $\angle\rho$ (Fig. 6). The relative relationship of the mean ROI value of $R_{VV/HH}$ and $|\rho|$ changes from scene to scene, hence no temporal consistency can be observed.

Sea ice relative permittivity is found to increase largely with increasing temperature as the sea ice temperature reaches above -7 to -5 °C (Vant, 1974; Barber et al., 1998). As the investigated scenes are all recorded at warm temperatures, a large variation in sea ice relative permittivity is expected between the scenes, even if the difference in air temperature between the scenes is relatively small. The temporal inconsistency of $R_{VV/HH}$ and $|\rho|$ may indicate a stronger sensitivity to relative permittivity of these two features. In Bragg-scattering theory $R_{VV/HH}$ is only dependent on the relative permittivity of the surface for a smooth surfaces (Fung, 1994). Based on differences in relative

Late summer sea ice segmentation with multi-polarisation SAR features in C- and X-band

A. S. Fors et al.

Title Page

Abstract

Introduction

Conclusions

References

Tables

Figures

◀

▶

◀

▶

Back

Close

Full Screen / Esc

Printer-friendly Version

Interactive Discussion



permittivity, FYI and old ice have been separated from saline young ice, leads and melt ponds by use of $R_{VV/HH}$ (see Scharien et al., 2014a, and references therein).

Another possible reason for the inconsistency of these two features is a stronger sensitivity to changes in incidence angles than for the rest of the features. Note that the incidence angle of the three RS-2 scenes varies between 38 and 48° (see Table 1). It is, however hard to reveal such a dependency from Fig. 6 for any of the features, indicating that the variation in mean ROI value of the features between the scenes is more dependent on other conditions, for instance air temperature and moisture at the site, than on the incidence angle.

Gill et al. (2013) did a study on feature temporal consistency in C-band between a winter and a spring scene on FYI north of Canada. They found, similar to this study, that $\angle\rho$ showed high consistency during changing temperature conditions. In contradiction to our findings, they also found $R_{VV/HH}$ to have high temporal consistency. RK and B were not included in their study. The differences in results may be explained by different incidence angles, sea ice types and snow conditions.

T2 shows similar relationships between the mean ROI values of the features as the RS-2 scenes for all three features extracted (Figs. 6 and 7). The same between-ROI relationship can not be found for T1. This may be due to the air temperature being above zero degrees Celcius at the time of acquisition of this specific scene. The error bars in the TS-X ROIs are in general larger than in the RS-2 ROIs, which may indicate slightly poorer discrimination ability of the TS-X scenes.

3.1.3 Feature set for late summer sea ice segmentation

At the time of the campaign, the melt season was about to end. In this period with air temperatures fluctuating around the zero degrees Celcius, small changes in atmospheric conditions could have large impact on the sea ice surface properties. SAR is sensitive to the large changes in relative permittivity connected to air temperatures close to zero degrees Celsius (Vant, 1974; Barber et al., 1998), and to variation in

Late summer sea ice segmentation with multi-polarisation SAR features in C- and X-band

A. S. Fors et al.

Title Page

Abstract

Introduction

Conclusions

References

Tables

Figures

◀

▶

◀

▶

Back

Close

Full Screen / Esc

Printer-friendly Version

Interactive Discussion



moisture content in the sea ice volume caused by freeze and thaw cycles (Scharien et al., 2010).

A sea ice segmentation algorithm for late summer sea ice is required to give consistent results during changing atmospheric conditions, as in situ information are often not available. Therefore, while searching for a suitable feature set for late summer sea ice segmentation, both the discrimination ability of the features and their temporally consistency are important. All features in our study showed some discrimination potential, but none could solely discriminate between all ROIs in our study. Combining several of the features may improve the classification accuracy. Four out of the six investigated features were found to be temporally consistent in the period investigated. Excluding temporally inconsistent features could help achieve a more temporally stable segmentation during changing atmospheric conditions. We therefore suggest a reduced feature set, consisting of RK , B , $R_{VH/VV}$ and $\angle\rho$ for late summer sea ice segmentation. A reduction of features in the feature set could of course also imply loss of important information and hence degradation in the segmentation performance. The following section will further explore the use of a reduced feature set.

3.2 Segmentation

In this section, the suitability of an automatic feature-based segmentation for late summer sea ice segmentation is tested. The segmentation is tested both with the full feature set including all six features investigated in this study (Table 3), and with a reduced feature set. The reduced feature set includes the features found to be the most temporally consistent in Sect. 3.1, hence $R_{VV/HH}$ and $|\rho|$ are excluded. We evaluate the performance of the segmentation visually, and by its ability to discriminate the five ROIs from each other.

Late summer sea ice segmentation with multi-polarisation SAR features in C- and X-band

A. S. Fors et al.

Title Page

Abstract

Introduction

Conclusions

References

Tables

Figures

◀

▶

◀

▶

Back

Close

Full Screen / Esc

Printer-friendly Version

Interactive Discussion



3.2.1 Segmentation performance

The segmented images for RS-2 are presented in Fig. 8, with the full feature set to the left and the reduced feature set to the right. The segmentations with the full feature set of R1 (Fig. 8a) and R2 (Fig. 8c) both look reasonable compared to the information from the helicopter flight. One can recognise the thin FYI ice area in the middle of the scenes (violet), the heavily deformed old ice areas in the diagonal bottom-left part of the scenes (blue and turquoise), and two different sea ice classes north and south of the middle region with thin FYI (orange and yellow). The segmentation with the full feature set of R3 (Fig. 8e) has a more granular appearance. However, the thin FYI area in the middle (violet) and the heavily deformed old ice areas in the bottom-left diagonal part of the scene (blue and turquoise) are well segmented. The areas with medium thick FYI north of the middle region, and the areas with old ice south of the middle region are confused (yellow, orange, grey). The differences between the segmentations with full and reduced feature sets for the three RS-2 scenes are in general small. The segmentation of R3 becomes slightly noisier with the reduced feature set (Fig. 8).

Figure 9 displays which classes the pixels of each of the ROIs are segmented to in all three RS-2 scenes, both for the full (left) and the reduced (right) feature sets. In general, the segmentations with the full feature set gives good distinction between the different ROIs included in this study. In particular, the thin FYI in ROI2 and the deformed old ice in ROI5 are separated with an accuracy above 71 % from the other ROIs in all of the three scenes. In R1 and R2 the segmentation is not able to separate ROI3 and ROI4 clearly (Fig. 9a and c). These ROIs do both contain old ice, with different thicknesses and melt pond fractions, hence the ice types in the ROIs are quite similar. In R3 the medium thick FYI in ROI1 is misclassified between several classes. Reducing the feature set by excluding the temporally inconsistent features does not affect the results for R1 and R2 (Fig. 9b and d). In R3, it improves the separation of medium thick FYI in ROI1, and reduces the discrimination between the thin FYI in ROI2 and the old ice in ROI3 (Fig. 9f).

Late summer sea ice segmentation with multi-polarisation SAR features in C- and X-band

A. S. Fors et al.

Title Page

Abstract

Introduction

Conclusions

References

Tables

Figures

◀

▶

◀

▶

Back

Close

Full Screen / Esc

Printer-friendly Version

Interactive Discussion

different incidence angles and resolutions, and the meteorological conditions are different (see Table 1 and Fig. 2). A drop in temperature and relative humidity prior to the acquisition of R3 could have caused rime on the sea ice surface (Drinkwater, 1995), or draining and refreezing of freshwater in the upper layers of the sea ice (Scharien et al., 2010). Both of which could cause a lower contrast between different sea ice types, and hence hamper the segmentation result.

The segmentation of the TS-X scenes with the full achievable feature set showed poor performance for T1. In T2, some important regions were well segmented, even with only three achievable features out of the six used in the RS-2 scenes. Reducing the feature set slightly improved the segmentation performance of T1. The backscatter intensity (VV) in T1 is in general more than five dB lower than that in T2, but still well above the noise floor. According to the meteorological measurements from Lance, T1 was acquired during a period with air temperatures above zero degree Celsius and high relative humidity (see Fig. 2). These conditions are probably at the limit of conditions suitable for sea ice type discrimination by SAR. As reported by Scharien et al. (2010), moisture in the upper sea ice layer could mask out volume scattering, and hence lower the backscatter contrast between different sea ice types. The meteorological conditions could explain the poor segmentation of T1. The improved segmentation of T1 with the reduced feature set could imply that the algorithm benefits from excluding temporally inconsistent features at air temperatures above zero degree Celsius

The poorer segmentation performance of the TS-X scenes, compared to the RS-2 scenes, is not necessarily a result of difference in frequency. Fewer polarisation channels, lower incidence angles, different resolution and different geophysical conditions at the time of the acquisition could all contribute to a poorer segmentation. More scenes are required to investigate the limitations of the segmentation algorithm with respect to the above mentioned factors.

Choice of sliding window size and number of classes are important for the segmentation results. The use of window size of 21×21 pixels or larger showed the best results in our dataset. The size of the window was in our case a trade-off between resolu-

tion details (small window) and segmentation with little speckle and larger continuous regions (large window). The number of classes was set in advance, based on visual inspection of the scenes and in situ information. Choosing too few classes could force different ice types into a common class, while increasing the number of classes could split an ice type into several classes.

4 Conclusions

This study examined the potential of sea ice segmentation by C- and X-band multi-polarisation SAR features during late summer in the Fram Strait. Firstly, the individual features sea ice type discrimination ability and their temporal consistency were investigated. Secondly, an automatic feature-based segmentation was tested.

The ability of the individual features to discriminate five sea ice types during changing temperature conditions was evaluated by a MAP supervised classifier, and by a qualitative study of the temporal consistency of the features. The classification results revealed a potential in all individual features for discriminating some of the sea ice types from each other, but none of the individual features could separate the total set of sea ice types in any of the scenes. Hence, a combination of the features has the potential of segmenting the different sea ice types included in our study. Temporal consistency was evaluated by studying the ability of the features to rank the mean value of the five sea ice types in the same order through the three RS-2 scenes. Relative kurtosis, geometric brightness, cross-polarisation ratio and co-polarisation correlation angle were found to give good temporal consistency during changing temperature conditions. These features were suggested as a reduced feature set. Co-polarisation ratio and co-polarisation correlation magnitude were found to be inconsistent through the period investigated. A possible reason for the two features inconsistency could be a higher sensitivity to changes in relative permittivity. Our study demonstrates some of the difficulties of sea ice type discrimination at temperatures close to zero degree Celcius, and highlights that it is important to cautiously select features for consistent sea ice monitor-

Late summer sea ice segmentation with multi-polarisation SAR features in C- and X-band

A. S. Fors et al.

Title Page

Abstract

Introduction

Conclusions

References

Tables

Figures



Back

Close

Full Screen / Esc

Printer-friendly Version

Interactive Discussion



ing during late summer. Our study shows as well that it is possible to retrieve valuable information from multi-polarisation SAR imagery, even under these difficult conditions.

An automatic feature-based segmentation algorithm was tested on the dataset and evaluated visually and through its ability to discriminate the five investigated sea ice types. The segmentation was tested for a full feature set of six features and for a reduced feature set of the four features showing best temporal consistency. The segmentation was in general performing well on the three RS-2 scenes. It showed good temporal consistency between the scenes, both for the full and for the reduced feature set. However, reducing the feature set did slightly degrade the segmentation performance of one of the scenes. The segmentation succeeded in segmenting some of the sea ice types in one of the two TS-X scenes. In the other scene the segmentation performed poorly, probably due to air temperatures above freezing point and hence difficult conditions for sea ice characterization by SAR. Reducing the feature set introduced a slight improvement in this poorest segmented scene. In total, the automatic feature-based segmentation algorithm demonstrates a potential of sea ice type discrimination during late summer, and our results indicate that an exclusion of temporal inconsistent features could improve the segmentation results when the temperature is close to or above freezing point. To confirm this, more scenes need to be investigated.

Both C- and X-band scenes were included in the study, but differences in incidence angles, resolution and number of polarisation channels made a direct comparison with respect to frequency inappropriate. One of the X-band scenes showed promising results when it came to sea ice type discrimination, close to those achieved for the quad polarimetric RS-2 scenes, even if it was a dual polarimetric scene. However investigations of more scenes with different incidence angle and polarisation combinations are necessary to reveal the potential of X-band in sea ice discrimination.

Future studies should also focus on a better physical understanding of the relation between SAR polarimetric features and geophysical properties which would be important for sea ice analysts to improve the interpretation and labeling of segmented sea ice scenes. The suitability of other features in late summer sea ice segmentation should

Late summer sea ice segmentation with multi-polarisation SAR features in C- and X-band

A. S. Fors et al.

Title Page

Abstract

Introduction

Conclusions

References

Tables

Figures



Back

Close

Full Screen / Esc

Printer-friendly Version

Interactive Discussion



Late summer sea ice segmentation with multi-polarisation SAR features in C- and X-band

A. S. Fors et al.

Title Page

Abstract

Introduction

Conclusions

References

Tables

Figures

◀

▶

◀

▶

Back

Close

Full Screen / Esc

Printer-friendly Version

Interactive Discussion

- Carlstrom, A. and Ulander, L.: C-band backscatter signatures of old sea ice in the central Arctic during freeze-up, *IEEE T. Geosci. Remote*, 31, 819–829, doi:10.1109/36.239904, 1993. 4542
- Dabboor, M. and Geldsetzer, T.: Towards sea ice classification using simulated RADARSAT Constellation Mission compact polarimetric SAR imagery, *Remote Sens. Environ.*, 140, 189–195, doi:10.1016/j.rse.2013.08.035, 2014. 4541
- DeCarlo, L. T.: On the meaning and use of kurtosis, *Psychol. Methods*, 2, 292–307, doi:10.1037/1082-989X.2.3.292, 1997. 4549
- Doulgeris, A. P.: A simple and extendable segmentation method for multi-polarisation SAR images, in: *Proc. of PolInSAR 2013, 6th International Workshop on Science and Applications of SAR Polarimetry and Polarimetric Interferometry*, 28 January–1 February 2013, Frascati, Italy, ESA SP-713, European Space Agency, Paris, 2013. 4542, 4551
- Doulgeris, A. P. and Eltoft, T.: Scale mixture of Gaussian modelling of polarimetric SAR data, *EURASIP J. Adv. Sig. Pr.*, 2010, 1–13, doi:10.1155/2010/874592, 2010. 4542, 4549
- Drinkwater, M.: *Airborne and satellite SAR investigations of sea-ice surface characteristics*, in: *Oceanographic Applications of Remote Sensing*, CRC Press, Boca Raton, Florida, 339–357, 1995. 4558
- Drinkwater, M., Kwok, R., Rignot, E., Israelsson, H., Onstott, R. G., and Winebrenner, D. P.: Potential applications of polarimetry to the classification of sea ice, in: *Microwave Remote Sensing of Sea Ice*, edited by: Carsey, F. D., vol. 68, Geophysical Monograph Series, American Geophysical Union, Washington, DC, 419–430, doi:10.1029/GM068, 1992. 4549
- Eriksson, L. E. B., Borena, K., Dierking, W., Berg, A., Santoro, M., Pemberton, P., Lindh, H., and Karlson, B.: Evaluation of new spaceborne SAR sensors for sea-ice monitoring in the Baltic Sea, *Can. J. Remote Sens.*, 36, S56–S73, 2010. 4541
- Fung, A. K.: *Microwave Scattering and Emission Models and their Applications*, Artech House Inc., Norwood, MA, 1994. 4553
- Gill, J. P., Yackel, J. J., and Geldsetzer, T.: Analysis of consistency in first-year sea ice classification potential of C-band SAR polarimetric parameters, *Can. J. Remote Sens.*, 39, 101–117, doi:10.5589/m13-016, 2013. 4542, 4554
- Gogineni, S. P., Moore, R. K., Grenfell, T. C., Barber, D. G., Digby, S., and Drinkwater, M.: The effects of freeze-up and melt processes on microwave signatures, in: *Microwave Remote Sensing of Sea Ice*, edited by: Carsey, F. D., vol. 68, American Geophysical Union, Washington, DC, 329–341, 1992. 4542

Late summer sea ice segmentation with multi-polarisation SAR features in C- and X-band

A. S. Fors et al.

Title Page

Abstract

Introduction

Conclusions

References

Tables

Figures

◀

▶

◀

▶

Back

Close

Full Screen / Esc

Printer-friendly Version

Interactive Discussion

- Haas, C., Lobach, J., Hendricks, S., Rabenstein, L., and Pfaffling, A.: Helicopter-borne measurements of sea ice thickness, using a small and lightweight, digital EM system, *J. Appl. Geophys.*, 67, 234–241, doi:10.1016/j.jappgeo.2008.05.005, 2009. 4545
- Hibler, W. D.: Removal of aircraft altitude variation from laser profiles of the arctic ice pack, *J. Geophys. Res.*, 77, 7190–7195, doi:10.1029/JC077i036p07190, 1972. 4545
- Isleifson, D., Langlois, A., Barber, D. G., and Shafai, L.: C-band scatterometer measurements of multiyear sea ice before fall freeze-up in the Canadian Arctic, *IEEE T. Geosci. Remote*, 47, 1651–1661, 2009. 4542
- Jeffries, M. O., Schwartz, K., and Li, S.: Arctic summer sea-ice SAR signatures, melt-season characteristics, and melt-pond fractions, *Polar Rec.*, 33, 101–112, doi:10.1017/S003224740001442X, 1997. 4542
- Kwok, R., Cunningham, G. F., Wensnahan, M., Rigor, I., Zwally, H. J., and Yi, D.: Thinning and volume loss of the Arctic Ocean sea ice cover: 2003–2008, *J. Geophys. Res.*, 114, C07005, doi:10.1029/2009JC005312, 2009. 4540
- Laxon, S. W., Giles, K. A., Ridout, A. L., Wingham, D. J., Willatt, R., Cullen, R., Kwok, R., Schweiger, A., Zhang, J., Haas, C., Hendricks, S., Krishfield, R., Kurtz, N., Farrell, S., and Davidson, M.: CryoSat-2 estimates of Arctic sea ice thickness and volume, *Geophys. Res. Lett.*, 40, 732–737, doi:10.1002/grl.50193, 2013. 4540
- Lee, J. S. and Pottier, E.: *Polarimetric radar imaging: from basics to applications*, CRC Press, Boca Raton, Florida, 2009. 4548
- Mäkynen, M. and Hallikainen, M.: Investigation of C- and X-band backscattering signatures of Baltic Sea ice, *Int. J. Remote Sens.*, 25, 37–41, doi:10.1080/01431160310001647697, 2004. 4541
- Mardia, K. V.: Measure of multivariate skewness and kurtosis with applications, *Biometrika*, 57, 519–530, 1970. 4549
- Matsuoka, T., Uratsuka, S., Satake, M., Kobayashi, T., Nadai, A., Umehara, T., Maeno, H., Wakabayashi, H., Nakamura, K., and Nishio, F.: CRL/NASDA airborne SAR (Pi-SAR) observations of sea ice in the Sea of Okhotsk, *Ann. Glaciol.*, 33, 115–119, 2001. 4541
- Meier, W. N., Hovelsrud, G. K., van Oort, B. E., Key, J. R., Kovacs, K. M., Michel, C., Haas, C., Granskog, M. A., Gerland, S., Perovich, D. K., Makshtas, A., and Reist, J. D.: Arctic sea ice in transformation: a review of recent observed changes and impacts on biology and human activity, *Rev. Geophys.*, 52, 185–217, doi:10.1002/2013RG000431, 2014. 4540

Late summer sea ice segmentation with multi-polarisation SAR features in C- and X-band

A. S. Fors et al.

Title Page

Abstract

Introduction

Conclusions

References

Tables

Figures

◀

▶

◀

▶

Back

Close

Full Screen / Esc

Printer-friendly Version

Interactive Discussion

- Moen, M.-A. N., Doulgeris, A. P., Anfinsen, S. N., Renner, A. H. H., Hughes, N., Gerland, S., and Eltoft, T.: Comparison of feature based segmentation of full polarimetric SAR satellite sea ice images with manually drawn ice charts, *The Cryosphere*, 7, 1693–1705, doi:10.5194/tc-7-1693-2013, 2013. 4541, 4542, 4543, 4548, 4549, 4551
- 5 Onstott, R. G.: SAR and scatterometer signatures of sea ice, in: *Microwave Remote Sensing of Sea Ice*, edited by: Carsey, F., vol. 68, American Geophysical Union, Washington, DC, 73–104, 1992. 4541, 4542
- Parkinson, C. L. and Comiso, J. C.: On the 2012 record low Arctic sea ice cover: combined impact of preconditioning and an August storm, *Geophys. Res. Lett.*, 40, 1356–1361, doi:10.1002/grl.50349, 2013. 4540
- 10 Pedersen, C. A., Hall, R., Gerland, S., Sivertsen, A., Svenøe, T., and Haas, C.: Combined airborne profiling over Fram Strait sea ice: fractional sea-ice types, albedo and thickness measurements, *Cold Reg. Sci. Technol.*, 55, 23–32, doi:10.1016/j.coldregions.2008.08.004, 2009. 4546
- 15 Raney, R. K.: Hybrid-polarity SAR architecture, *IEEE T. Geosci. Remote*, 45, 3397–3404, 2007. 4541
- Renner, A. H. H., Dumont, M., Beckers, J., Gerland, S., and Haas, C.: Improved characterisation of sea ice using simultaneous aerial photography and sea ice thickness measurements, *Cold Reg. Sci. Technol.*, 92, 37–47, doi:10.1016/j.coldregions.2013.03.009, 2013. 4545, 4546
- 20 Renner, A. H. H., Gerland, S., Haas, C., Spreen, G., Beckers, J. F., Hansen, E., Nicolaus, M., and Goodwin, H.: Evidence of Arctic sea ice thinning from direct observations, *Geophys. Res. Lett.*, 2012, 1–8, doi:10.1002/2014GL060369, 2014. 4545
- Scharien, R. K., Geldsetzer, T., Barber, D. G., Yackel, J. J., and Langlois, A.: Physical, dielectric, and C band microwave scattering properties of first-year sea ice during advanced melt, *J. Geophys. Res.*, 115, C12026, doi:10.1029/2010JC006257, 2010. 4555, 4558
- 25 Scharien, R. K., Yackel, J. J., Barber, D. G., Asplin, M., Gupta, M., and Isleifson, D.: Geophysical controls on C band polarimetric backscatter from melt pond covered Arctic first-year sea ice: Assessment using high-resolution scatterometry, *J. Geophys. Res.*, 117, C00G18, doi:10.1029/2011JC007353, 2012. 4542
- 30 Scharien, R. K., Landy, J., and Barber, D. G.: First-year sea ice melt pond fraction estimation from dual-polarisation C-band SAR – Part 1: In situ observations, *The Cryosphere*, 8, 2147–2162, doi:10.5194/tc-8-2147-2014, 2014a. 4554

Late summer sea ice segmentation with multi-polarisation SAR features in C- and X-band

A. S. Fors et al.

Title Page

Abstract

Introduction

Conclusions

References

Tables

Figures

◀

▶

◀

▶

Back

Close

Full Screen / Esc

Printer-friendly Version

Interactive Discussion



Scharien, R. K., Hochheim, K., Landy, J., and Barber, D. G.: First-year sea ice melt pond fraction estimation from dual-polarisation C-band SAR – Part 2: Scaling in situ to Radarsat-2, *The Cryosphere*, 8, 2163–2176, doi:10.5194/tc-8-2163-2014, 2014b. 4542

Stephenson, S. R., Smith, L. C., Brigham, L. W., and Agnew, J. A.: Projected 21st-century changes to Arctic marine access, *Climatic Change*, 118, 885–899, doi:10.1007/s10584-012-0685-0, 2013. 4541

Stroeve, J. C., Markus, T., Boisvert, L., Miller, J., and Barrett, A.: Changes in Arctic melt season and implications for sea ice loss, *Geophys. Res. Lett.*, 41, 1216–1225, doi:10.1002/2013GL058951, 2014. 4540

Theodoridis, S. and Koutroumbas, K.: *Pattern Recognition*, Academic Press, London, 2009. 4550

Vant, M. R.: Dielectric properties of fresh and sea ice at 10 and 35 GHz, *J. Appl. Phys.*, 45, 4712, doi:10.1063/1.1663123, 1974. 4553, 4554

von Saldern, C., Haas, C., and Dierking, W.: Parameterization of Arctic sea-ice surface roughness for application in ice type classification, *Ann. Glaciol.*, 44, 224–230, 2006. 4545

Warner, K., Iacozza, J., Scharien, R., and Barber, D.: On the classification of melt season first-year and multi-year sea ice in the Beaufort Sea using Radarsat-2 data, *Int. J. Remote Sens.*, 34, 3760–3774, doi:10.1080/01431161.2012.760855, 2013. 4542

World Meteorological Organisation: *Sea-ice nomenclature and interational system of sea ice symbols*, Tech. rep., World Meteorological Organisation, Geneva, Switzerland, 1989. 4547

Yackel, J. J. and Barber, D. G.: Melt ponds on sea ice in the Canadian Archipelago: 2. On the use of RADARSAT-1 synthetic aperture radar for geophysical inversion, *J. Geophys. Res.*, 105, 22061, doi:10.1029/2000JC900076, 2000. 4542

Late summer sea ice segmentation with multi-polarisation SAR features in C- and X-band

A. S. Fors et al.

Table 1. Overview of the data set.

Date	Time (UTC)	Scene ID	Satellite, mode and polarisation	Incidence angle (°)	Pixel spacing (m) (azimuth × slant range)
29 Aug 2011	17:41	R1	Radarsat-2, Fine Quad, HH,HV,VH,VV	38.2°	5.0 m × 5.0 m
30 Aug 2011	18:23	T1	TerraSAR-X, StripMap, HH,VV	29.4°	2.4 m × 1.9 m
31 Aug 2011	18:23	R2	Radarsat-2, Fine Quad, HH,HV,VH,VV	48.2°	4.7 m × 5.1 m
3 Sep 2011	14:09	–	Helicopter flighth	–	–
4 Sep 2011	18:07	R3	Radarsat-2, Fine Quad, HH,HV,VH,VV	44.4°	5.1 m × 6.8 m
5 Sep 2011	17:00	T2	TerraSAR-X, StripMap, VH,VV	25.9°	2.3 m × 2.1 m

Title Page

Abstract

Introduction

Conclusions

References

Tables

Figures

◀

▶

◀

▶

Back

Close

Full Screen / Esc

Printer-friendly Version

Interactive Discussion

Late summer sea ice segmentation with multi-polarisation SAR features in C- and X-band

A. S. Fors et al.

Table 2. Detailed information about the regions of interest (ROIs) from helicopter-borne measurements and the corresponding sea ice class labels (WMO nomenclatura).

ROI ID	Mean (modal) sea ice thickness (m)	Mean melt pond fraction (%)	Surface roughness, R_q (m)	Sea ice class labels
ROI1	1.3 (1.2) m	17 %	0.098 m	Medium thick first year ice
ROI2	0.6 (0.6) m	38 %	0.062 m	Thin first year ice
ROI3	2.1 (2.0) m	26 %	0.231 m	Old ice
ROI4	3.7 (3.3) m	11 %	0.204 m	Old ice
ROI5	11.7 (8.9) m	3 %	0.575 m	Old ice

Title Page

Abstract

Introduction

Conclusions

References

Tables

Figures

◀

▶

◀

▶

Back

Close

Full Screen / Esc

Printer-friendly Version

Interactive Discussion

Late summer sea ice segmentation with multi-polarisation SAR features in C- and X-band

A. S. Fors et al.

Table 3. Polarimetric SAR features included in the study.

Polarimetric feature	Definition	Extracted for scene
Relative kurtosis	$RK = \frac{1}{L} \frac{1}{d(d+1)} \sum_{i=1}^L [\mathbf{s}_i^* \mathbf{C}^{-1} \mathbf{s}_i]^2$	All scenes
Geometric brightness	$B = \sqrt[d]{\det(\mathbf{C})}$	All scenes
Cross-polarisation ratio	$R_{VH/VV} = \frac{\langle S_{VH} S_{VH}^* \rangle}{\langle S_{VV} S_{VV}^* \rangle}$	R1, R2, R3, T2
Co-polarisation ratio	$R_{VV/HH} = \frac{\langle S_{VV} S_{VV}^* \rangle}{\langle S_{HH} S_{HH}^* \rangle}$	R1, R2, R3, T1
Co-polarisation correlation magnitude	$ \rho = \left \frac{\langle S_{HH} S_{VV}^* \rangle}{\sqrt{\langle S_{HH} S_{HH}^* \rangle \langle S_{VV} S_{VV}^* \rangle}} \right $	R1, R2, R3, T1
Co-polarisation correlation angle	$\angle \rho = \angle (\langle S_{HH} S_{VV}^* \rangle)$	R1, R2, R3, T1

Title Page

Abstract

Introduction

Conclusions

References

Tables

Figures

◀

▶

◀

▶

Back

Close

Full Screen / Esc

Printer-friendly Version

Interactive Discussion

Table 4. Classification accuracy of individual polarimetric features in the three Radarsat-2 scenes derived from MAP classification. The best result for each ROI and the best overall accuracy for each scene are highlighted in bold.

Scene ID	Feature	Sea ice type classification accuracy (%)				
		ROI1	ROI2	ROI3	ROI4	ROI5
R1	RK	5	22	42	0	64
	<i>B</i>	1	69	71	10	78
	$R_{VH/VV}$	23	0	38	0	51
	$R_{VV/HH}$	7	49	15	0	40
	$ \rho $	0	41	31	5	46
	$\angle\rho$	0	30	70	0	41
R2	RK	41	28	0	7	8
	<i>B</i>	31	63	75	32	23
	$R_{VH/VV}$	19	87	0	18	44
	$R_{VV/HH}$	0	70	40	0	26
	$ \rho $	57	0	0	0	34
	$\angle\rho$	5	11	19	27	44
R3	RK	0	20	60	40	55
	<i>B</i>	38	45	24	26	54
	$R_{VH/VV}$	3	40	2	40	74
	$R_{VV/HH}$	61	35	0	41	0
	$ \rho $	31	50	6	2	58
	$\angle\rho$	14	0	0	23	51

Late summer sea ice segmentation with multi-polarisation SAR features in C- and X-band

A. S. Fors et al.

Title Page

Abstract

Introduction

Conclusions

References

Tables

Figures

◀

▶

◀

▶

Back

Close

Full Screen / Esc

Printer-friendly Version

Interactive Discussion



Late summer sea ice segmentation with multi-polarisation SAR features in C- and X-band

A. S. Fors et al.

Table 5. Classification accuracy of individual polarimetric features in the two TerraSAR-X scenes derived from MAP classification. The best result for each ROI in each scene is highlighted in bold.

Scene ID	Feature	Sea ice type classification accuracy (%)			
		ROI1	ROI2	ROI3	ROI4
T1	RK	35	3	24	17
	<i>B</i>	54	0	21	60
	$R_{VV/HH}$	54	17	16	19
	$ \rho $	51	44	0	19
	$\angle\rho$	59	12	22	18
T2	RK	44	0	32	6
	<i>B</i>	41	23	59	10
	$R_{VH/VV}$	16	61	19	23

Title Page

Abstract

Introduction

Conclusions

References

Tables

Figures

◀

▶

◀

▶

Back

Close

Full Screen / Esc

Printer-friendly Version

Interactive Discussion

Late summer sea ice segmentation with multi-polarisation SAR features in C- and X-band

A. S. Fors et al.

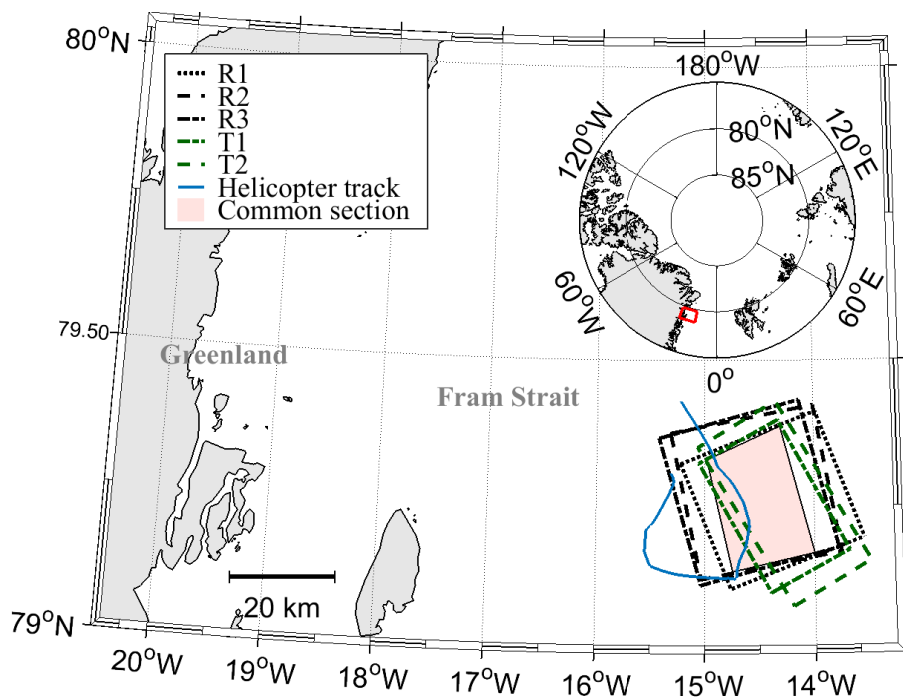


Figure 1. Map of the western Fram Strait showing the location of the satellite scenes included in the study and the track of the helicopter flight collecting airborne measurements for the study. The red box in the inset map of the Northern Hemisphere displays the geographical position of the area displayed. At the time of the flight, R/V *Lance* was slightly north of this map section.

Title Page

Abstract

Introduction

Conclusions

References

Tables

Figures

◀

▶

◀

▶

Back

Close

Full Screen / Esc

Printer-friendly Version

Interactive Discussion

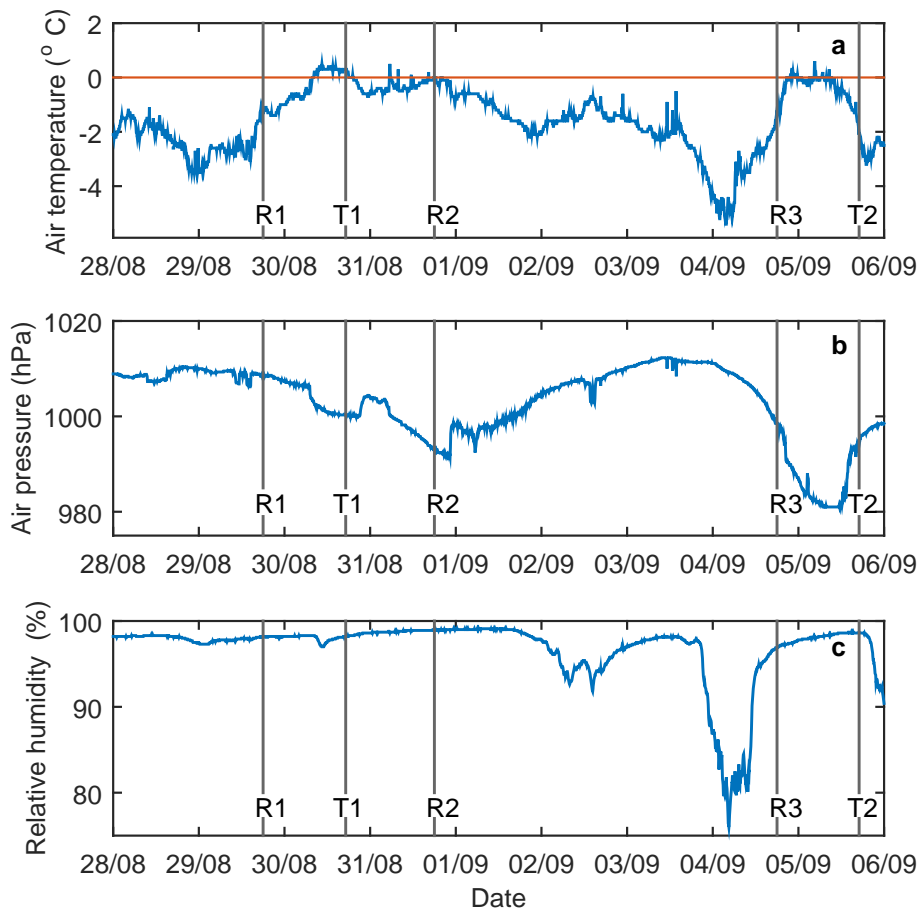


Figure 2. Air temperature (a), air pressure (b) and relative humidity (c) during the campaign. The gray vertical lines represent the time of the acquisition of the satellite scenes.

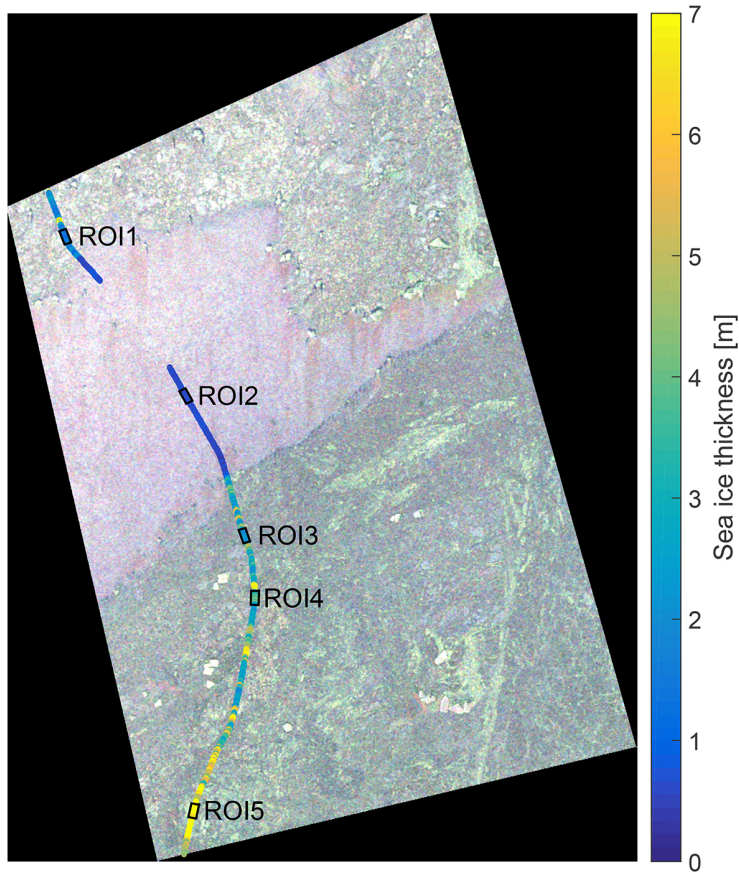


Figure 3. Position of regions of interest and helicopter thickness measurements displayed on the Radarsat-2 scene from 31 August 2011 (R2). The polarimetric image is a Pauli composite, the intensity channel combinations $|HH - VV|$, $2|HV|$ and $|HH + VV|$ are assigned to the red, green and blue (RGB) channels, respectively.

Late summer sea ice segmentation with multi-polarisation SAR features in C- and X-band

A. S. Fors et al.

Title Page

Abstract Introduction

Conclusions References

Tables Figures

◀ ▶

◀ ▶

Back Close

Full Screen / Esc

Printer-friendly Version

Interactive Discussion



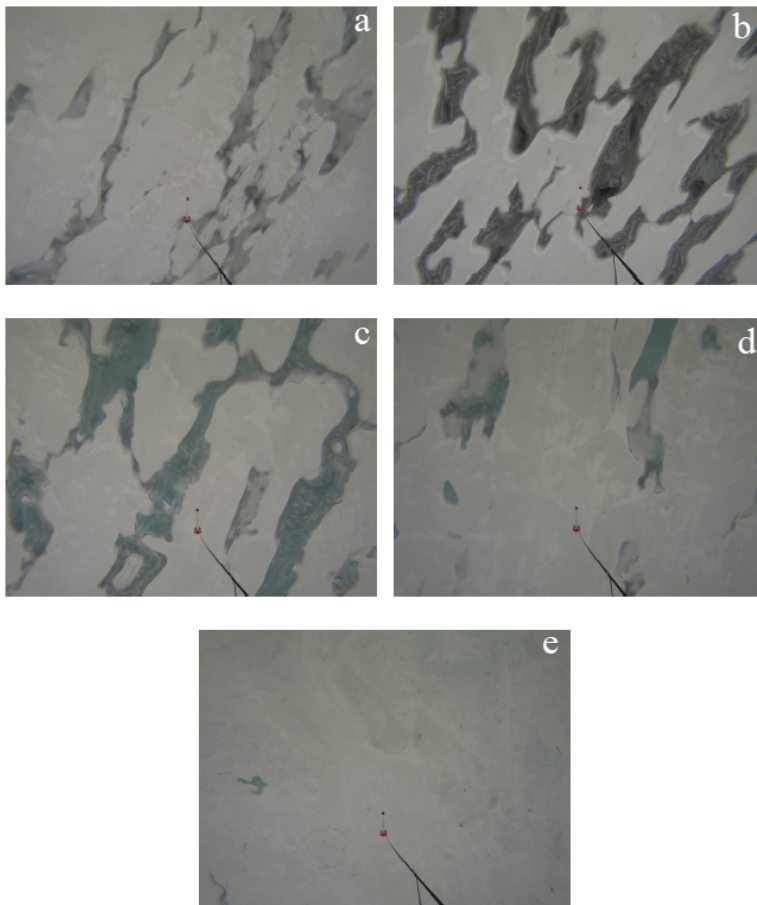


Figure 4. Example photos from the five regions of interest: **(a)** ROI1, **(b)** ROI2, **(c)** ROI3, **(d)** ROI4 and **(e)** ROI5. The photos are captured during the helicopter flight on 3 September 2011, and the EM-bird can be seen in the lower center part of each photo.

Late summer sea ice segmentation with multi-polarisation SAR features in C- and X-band

A. S. Fors et al.

Title Page

Abstract

Introduction

Conclusions

References

Tables

Figures

◀

▶

◀

▶

Back

Close

Full Screen / Esc

Printer-friendly Version

Interactive Discussion



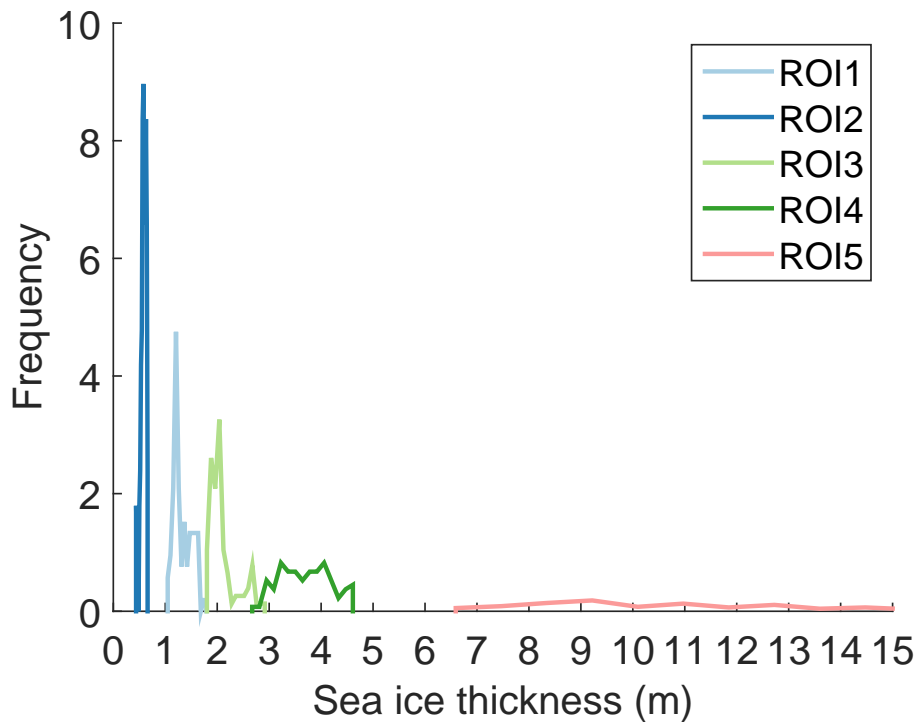


Figure 5. Histograms of sea ice thickness (m) measured during the helicopter flight 3 September 2011 for each of the five regions of interest.

Late summer sea ice segmentation with multi-polarisation SAR features in C- and X-band

A. S. Fors et al.

Title Page	
Abstract	Introduction
Conclusions	References
Tables	Figures
◀	▶
◀	▶
Back	Close
Full Screen / Esc	
Printer-friendly Version	
Interactive Discussion	



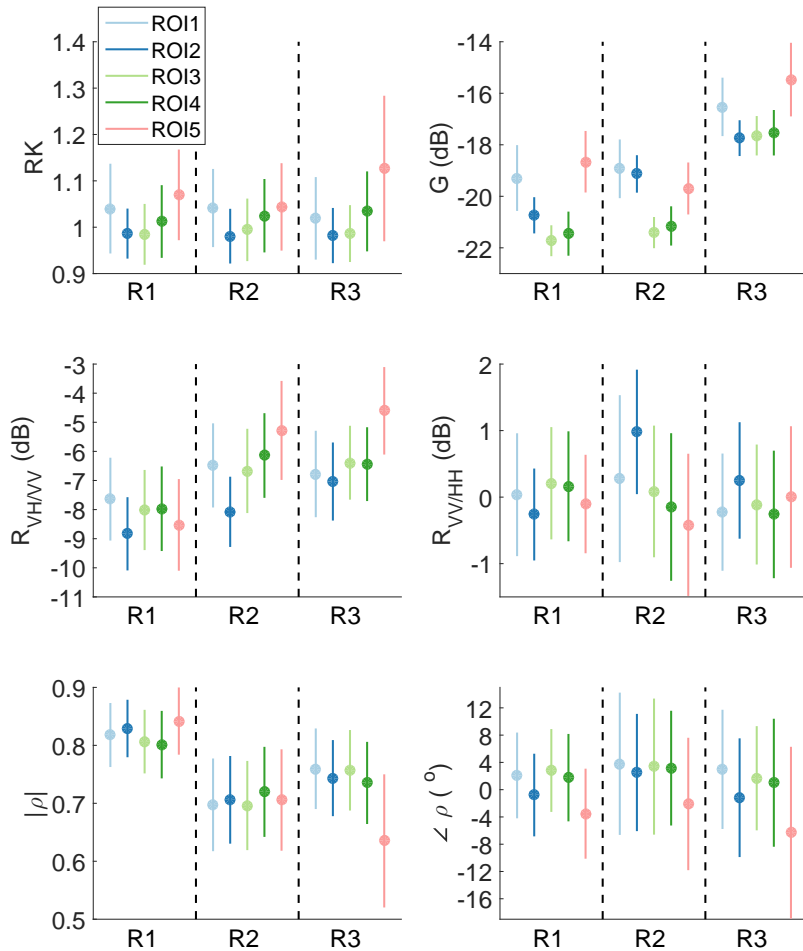


Figure 6. Mean values of the features in the regions of interest in the three Radarsat-2 scenes (R1, R2 and R3). The error bars are two standard deviations long.

Late summer sea ice segmentation with multi-polarisation SAR features in C- and X-band

A. S. Fors et al.

Title Page

Abstract Introduction

Conclusions References

Tables Figures

◀ ▶

◀ ▶

Back Close

Full Screen / Esc

Printer-friendly Version

Interactive Discussion



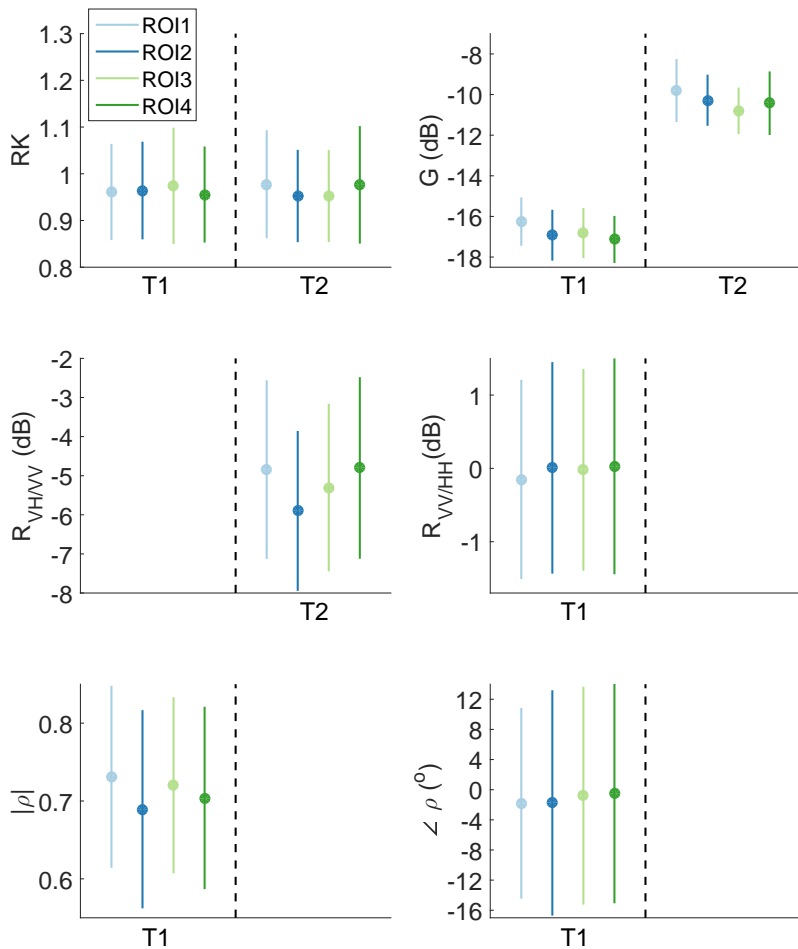


Figure 7. Mean values of the features in the regions of interest in the two TerraSAR-X scenes (T1 and T2). The error bars are two standard deviations long.

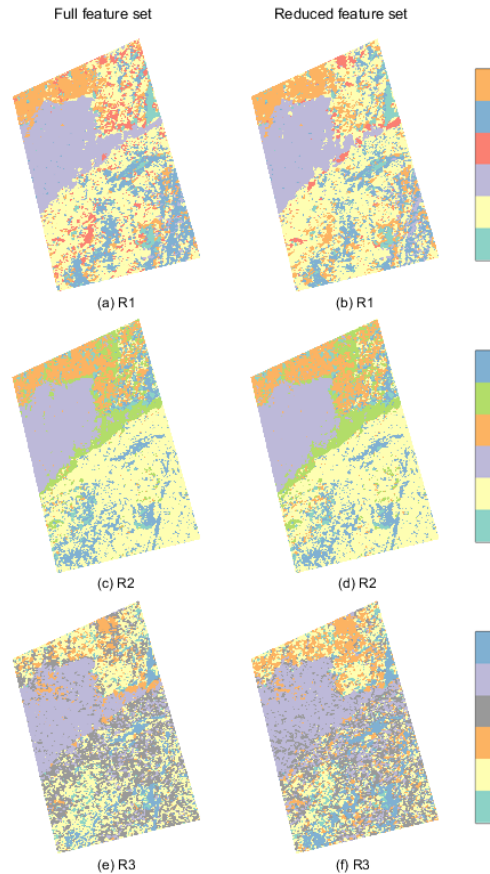


Figure 8. Segmentations of the three Radarsat-2 scenes (R1, R2 and R3) into six classes. To the left: segmentation with full feature set. To the right: segmentation with reduced feature set consisting of relative kurtosis, geometric brightness, cross-polarisation ratio and co-polarisation angle.

Late summer sea ice segmentation with multi-polarisation SAR features in C- and X-band

A. S. Fors et al.

Title Page

Abstract Introduction

Conclusions References

Tables Figures

◀ ▶

◀ ▶

Back Close

Full Screen / Esc

Printer-friendly Version

Interactive Discussion



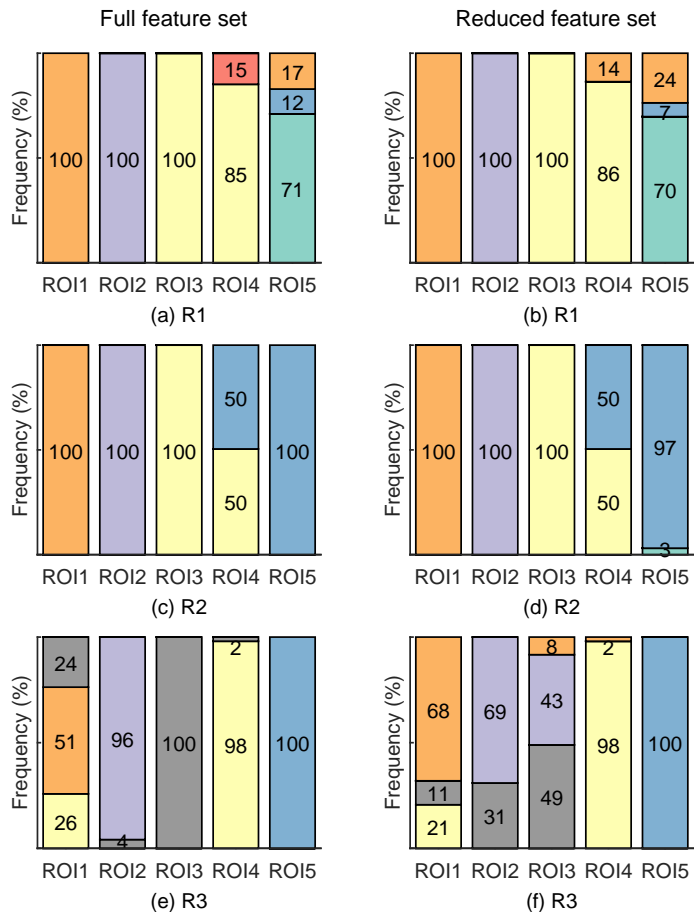


Figure 9. The classes assigned to the pixels in the five regions of interest by the segmentation of the three Radarsat-2 scenes (R1, R2 and R3). To the left: segmentation with full feature set. To the right: segmentation with reduced feature set.

Title Page

Abstract Introduction

Conclusions References

Tables Figures

◀ ▶

◀ ▶

Back Close

Full Screen / Esc

Printer-friendly Version

Interactive Discussion

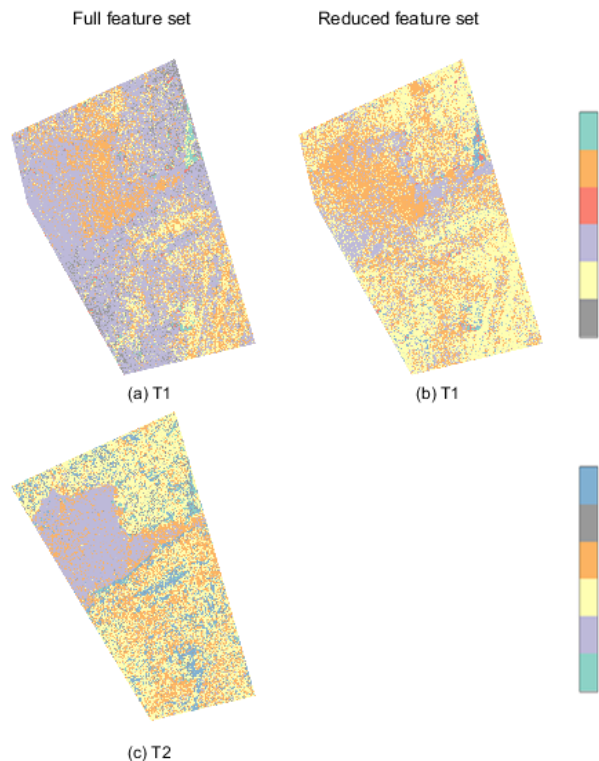


Figure 10. Segmentations of the two TerraSAR-X scenes (T1 and T2) into six classes. To the left: segmentation with full achievable feature set. For T1 the feature set consists of relative kurtosis, geometric brightness, co-polarisation ratio, co-polarisation correlation magnitude and co-polarisation correlation angle. For T2 the feature set consists of relative kurtosis, geometric brightness and cross-polarisation ratio. To the right: segmentation of T1 with the reduced feature set consisting of relative kurtosis, geometric brightness and co-polarisation correlation angle.

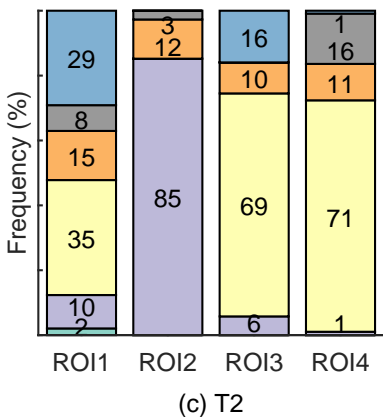
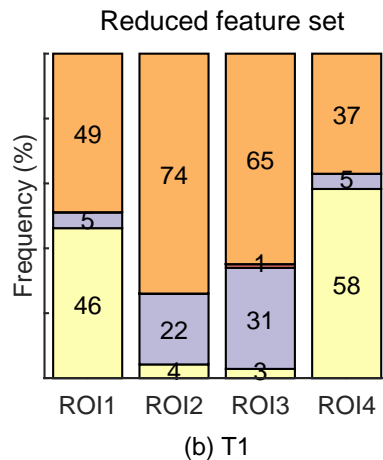
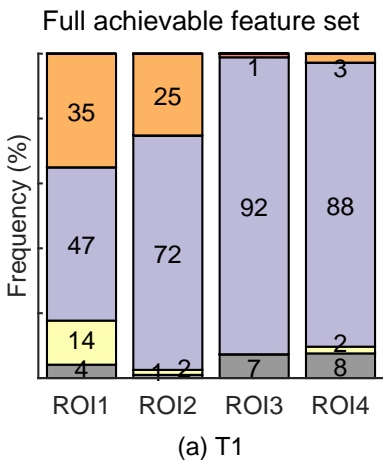


Figure 11. The classes assigned to the pixels in the five regions of interest by the segmentation of the two TerraSAR-X scenes (T1 and T2). To the left: segmentation of T1 and T2 with full achievable feature set. To the right: segmentation of T1 with reduced feature set.